

## DENSITY MATRIX ESTIMATION IN QUANTUM HOMODYNE TOMOGRAPHY

Yazhen Wang and Chenliang Xu

*University of Wisconsin-Madison*

*Abstract:* Modern scientific studies often involve complex quantum systems, and scientists need to learn the systems from experimental data. As density matrices are usually employed to characterize the quantum states of the systems, this paper investigates estimation of density matrices. We propose statistical methodologies to construct density matrix estimators and establish an asymptotic theory for the estimation methods. We show that the proposed density matrix estimators are consistent and have good convergence rates. A numerical study is conducted to demonstrate the finite sample performances of the proposed estimators.

*Key words and phrases:* Convergence rate, density matrix, large matrix estimation, quantum system, quantum tomography, spectral norm.

### 1. Introduction

Learning and manipulating quantum systems plays an important role in such scientific studies as quantum computation and quantum information. A quantum system is generally characterized by its state and the time evolution of the state, and it is important, but difficult, to know its state. We often conduct experiments in a laboratory to perform measurements on the quantum system and then infer the quantum state from the experimental data. Mathematically the quantum state can be described by a matrix called the density matrix of the quantum system. The problem can be formulated as a statistical problem of estimating the density matrix based on repeated measurements on quantum systems that are identically prepared in the state to be estimated. After obtaining measurements on some identical quantum systems we can make statistical inference about the probability distribution of the measurements, and thus indirectly about the density matrix of the quantum system. In the literature of quantum physics and quantum information science, this is referred to as quantum state tomography, the reconstruction of the density matrix by probing identically prepared quantum systems.

Density matrix estimation methods in physics usually focus on estimating individual matrix elements without studying the accuracy of a density matrix estimator as a whole matrix. With the introduction of quantum statistics by

Barndorff-Nielsen, Gill, and Jupp (2003) Artiles, Gill, and Guță (2005) proposed a sieve estimator of the density matrix and proved its consistency under trace and Frobenius norms. Guță and Artiles (2007) and Butucea, Guță, and Artiles (2007) investigated minimax estimation of the Wigner function (which characterizes a density matrix via a transformation) for noiseless data and noisy data, respectively, and proposed kernel estimators to achieve optimality. This paper investigates density matrix estimation for an infinite dimensional quantum system. Using the relationship between a density matrix and its corresponding density function of measurements we construct unbiased estimators of the entries of the density matrix; employing a regularization methodology developed for large matrix estimation we propose new estimators of the density matrix and, under a matrix sparsity assumption, we establish asymptotic theory for the proposed estimators. We show that the estimators are consistent and achieve high convergence rates under the spectral norm. We conduct a simulation study to illustrate the finite sample performances of the proposed estimators.

The rest of the paper proceeds as follows. Section 2 briefly reviews quantum mechanics. Section 3 presents density matrix estimation and establishes an asymptotic theory for the proposed density matrix estimators. Section 4 provides a simulation study to illustrate the finite sample performances of the proposed density matrix estimators. Section 5 features concluding remarks. The proofs are collected in Web Appendix.

## 2. Brief Review on Quantum Mechanics

Quantum mechanics describes phenomena at microscopic level. The theory of quantum mechanics provides a mathematical description of the states and the time evolutions of physical particle systems. Quantum theory is intrinsically stochastic in that we can only statistically predict quantum measurement results. Mathematically the theory is described by a Hilbert space  $\mathcal{H}$  and Hermitian (or self-adjoint) operators on  $\mathcal{H}$ .

A quantum system of particles is described by its state and the time evolution of the state. The quantum state can be characterized by a density matrix (or density operator)  $\rho$  on  $\mathcal{H}$ , which is self-adjoint, semi-positive, and unit trace. Thus, (1)  $\rho$  is equal to its adjoint  $(\rho^*)^\dagger$ , where we denote by  $*$  and  $\dagger$  conjugate and transpose operations, respectively; (2)  $\langle \mathbf{u}, \rho \mathbf{u} \rangle \geq 0$  for  $\mathbf{u} \in \mathcal{H}$ ; (3)  $Tr(\rho) = 1$ . Here we follow the convention in quantum information science to reserve notation  $\rho$  for a state or density matrix.

Measurements for a quantum system are obtained by laboratory experiments performed on the system. They are described through observables as follows, where an observable  $\mathbf{X}$  is defined as a self-adjoint operator on  $\mathcal{H}$ . Assume that  $\mathbf{X}$  has a spectral decomposition with real eigenvalues  $X_a$  and the corresponding

eigen-spaces  $\mathbf{Q}_a$ , where  $a$  belongs to some index set (which may be a discrete set or a continuous interval). When a laboratory experiment performs measurements on the observable  $\mathbf{X}$  for the quantum system prepared in state  $\rho$ , the resulting measurements are random and take values from the eigenvalues of  $\mathbf{X}$ , and the probability of observing a particular eigenvalue  $X_a$  as a measurement is equal to  $Tr(\rho\mathbf{Q}_a)$ . See Holevo (1982), Sakurai (1995) and Wang (2012).

### 3. Density Matrix Estimation

#### 3.1. Density matrix

An important quantum study involves measurements on position and momentum (or electric and magnetic fields) of a particle. Two central observables in the study are described by self-adjoint operators  $\mathbf{U}$  and  $\mathbf{V}$ , respectively, on Hilbert space  $\mathcal{H} = L^2(\mathbb{R})$ ,

$$[\mathbf{U} f](x) = x f(x), \quad [\mathbf{V} g](x) = -i \frac{dg(x)}{dx},$$

where  $L^2(\mathbb{R})$  denotes the space of square integrable complex valued functions on  $\mathbb{R}$ ,  $i = \sqrt{-1}$ , and  $f(x)$  and  $g(x)$  are two arbitrary functions in  $\mathcal{H}$ . The quantum system is described by  $\mathcal{H}$  and a state  $\rho$ , which is represented by a semi-positive, unit trace, infinite matrices, with elements  $\rho_{j\ell} = \langle e_j, \rho e_\ell \rangle$ ,  $j, \ell = 1, 2, \dots$ , where  $\mathbf{e} = \{e_1, e_2, \dots\}$  is an orthonormal basis in  $\mathcal{H}$ . The quantum system has a long history and is extremely important in quantum physics, and a technique called quantum homodyne tomography in quantum optics has been developed to perform measurements on observables  $\mathbf{U}$  and  $\mathbf{V}$ . Such physical quantum systems are typically light pulses, and the goal of quantum engineering experiments is often to create some interesting states of light for the research and application studies in quantum computation, quantum information and quantum cryptography. To verify the creation of a state experimentalists need to perform measurements on observables  $\mathbf{U}$  and  $\mathbf{V}$  for the quantum system. However,  $\mathbf{U}$  and  $\mathbf{V}$  do not commute, in fact,  $\mathbf{U}$  and  $\mathbf{V}$  satisfy Heisenberg’s commutation relation  $\mathbf{U}\mathbf{V} - \mathbf{V}\mathbf{U} = i\mathbf{I}$ , thus they cannot be measured simultaneously. The quantum homodyne detection technique produces samples from the marginal of  $\mathbf{U}$  and  $\mathbf{V}$  along various chosen directions. For this reason the state reconstruction is known as quantum homodyne tomography.

Quantum homodyne tomography is able to measure the so-called quadrature observables  $\mathbf{X}_\phi = \mathbf{U} \cos \phi + \mathbf{V} \sin \phi$  for any phase directions  $\phi$ . Once performing measurements on  $\mathbf{X}_\phi$  for a sufficient number of quantum systems identically prepared under the state  $\rho$ , we estimate  $\rho$  from the acquired random measurement data. In the experiment  $\phi$  is chosen to be uniformly distributed on the interval  $[0, \pi]$  and independent of  $(\mathbf{U}, \mathbf{V})$ . For  $n$  quantum systems prepared in

the same state  $\rho$ , we measure quadratures  $\mathbf{X}_{\phi_k}$  on the  $k$ -th system with phase  $\phi_k$  selected independently from a uniform distribution on  $[0, \pi]$  and obtain independent identically distributed random variables  $(X_{\phi_1}, \phi_1), \dots, (X_{\phi_n}, \phi_n)$ , quantum measurement results of observables  $\mathbf{X}_\phi$ . Our goal is to estimate density matrix  $\rho$  based on  $(X_{\phi_1}, \phi_1), \dots, (X_{\phi_n}, \phi_n)$ .

Following the literature we take the Hermite polynomials normalized by  $\exp(-x^2/2)$  as an orthonormal basis  $\mathbf{e} = \{e_1, e_2, \dots\}$  in  $\mathcal{H}$  and obtain an infinite density matrix  $\rho = (\rho_{j\ell})$  for the quantum system. Denote by  $h_\rho(x, \phi)$  the joint probability density function (pdf) of  $(X_{\phi_k}, \phi_k)$ . We obtain measurements  $(X_{\phi_k}, \phi_k)$  performing on  $\mathbf{X}_\phi$  with probability dictated by the eigen-structure of  $\mathbf{X}_\phi$  and the state  $\rho$  of the quantum system. Thus, the pdf  $h_\rho(x, \phi)$  of the measurements on observables  $\mathbf{X}_{\phi_k}$  must be related to state  $\rho$ . Indeed, we have deep relationship between  $h_\rho(x, \phi)$  and  $\rho = (\rho_{j\ell})$ ,

$$h_\rho(x, \phi) = \frac{1}{\pi} \sum_{j, \ell=1}^{\infty} \rho_{j\ell} e_j(x) e_\ell(x) e^{-i(j-\ell)\phi}, \quad (3.1)$$

$$\rho_{j\ell} = \int_{-\infty}^{\infty} dx \int_0^\pi \frac{d\phi}{\pi} h_\rho(x, \phi) f_{j\ell}(x) e^{-i(j-\ell)\phi}, \quad (3.2)$$

where  $f_{j\ell}(x)$  are known bounded real-valued functions called pattern functions. The pattern functions  $f_{j\ell}(x)$  have oscillatory parts concentrating around zero with the lengths of the oscillatory parts and the numbers of oscillations increasing with  $j$  and  $\ell$ , and their tails decaying like  $x^{-2-|j-\ell|}$ . See D'Ariano, Leonhardt, and Paul (1995) Leonhardt, Paul, and D'Ariano (1995) and Leonhardt et al. (1996) for details on deriving the relationship.

### 3.2. Estimation

Since  $h_\rho(x, \phi)$  is the joint pdf of random variable  $(\phi, X_\phi)$ , we can rewrite (3.2) as

$$\rho_{j\ell} = E[F_{j\ell}(X_\phi, \phi)], \quad F_{j\ell}(x, \phi) = f_{j\ell}(x) e^{-i(j-\ell)\phi}, \quad (3.3)$$

where the expectation is taken with respect to the pdf  $h_\rho(x, \phi)$  of  $(X_\phi, \phi)$ . This leads to an unbiased estimator of each entry  $\rho_{j\ell}$  as

$$\bar{\rho}_{j\ell} = \frac{1}{n} \sum_{k=1}^n F_{j\ell}(X_{\phi_k}, \phi_k), \quad j, \ell \geq 1. \quad (3.4)$$

The true density matrix  $\rho$  is a semi-positive definite, unit trace matrix of infinite size, with entries  $\rho_{j\ell}$  that must decay as  $j$  and/or  $\ell$  go to infinity. To estimate  $\rho$  based on finite observations, we need to truncate the infinity matrix  $\rho$  by its first  $p$  rows and columns for some integer  $p$  and construct a density matrix estimator of size  $p$  to estimate  $(\rho_{j\ell})_{1 \leq j, \ell \leq p}$ .

For each entry,  $\bar{\rho}_{j\ell}$  can consistently estimate  $\rho_{j\ell}$ . However, as a matrix estimator of  $(\rho_{j\ell})_{1 \leq j, \ell \leq p}$ ,  $(\bar{\rho}_{j\ell})_{1 \leq j, \ell \leq p}$  performs poorly for large  $p$  even when  $n$  gets very large, let alone give consistent estimation of the infinite matrix  $(\rho_{j\ell})_{j, \ell \geq 1}$ . It is well documented that matrix estimators like  $(\bar{\rho}_{j\ell})_{1 \leq j, \ell \leq p}$  are inconsistent when  $n$  and  $p$  both go to infinity (see Bickel and Levina (2008), Cai and Zhou (2012), Tao, Wang, and Zhou (2013), and Wang and Zou (2010)). Fortunately large matrices often have some structures, such as sparsity, and we can regularize matrix estimator  $(\bar{\rho}_{j\ell})_{1 \leq j, \ell \leq p}$  to yield a consistent matrix estimator of  $(\rho_{j\ell})_{1 \leq j, \ell \leq p}$ . Under some proper bases density matrices often have sparse representations in a sense that each row (or column) has a relatively small portion of entries with large magnitude. Our strategy is to identify and estimate these large entries and ignore the small entries. We use the threshold method to construct a matrix estimator of  $\rho$  as

$$\hat{\rho} = (\hat{\rho}_{j\ell}), \hat{\rho}_{j\ell} = \mathcal{T}_\varpi[\bar{\rho}_{j\ell}] \text{ for } j, \ell \leq p \text{ and } \hat{\rho}_{j\ell} = 0 \text{ for } j > p \text{ or } \ell > p, \quad (3.5)$$

where for the soft threshold rule,

$$\mathcal{T}_\varpi[\bar{\rho}_{j\ell}] = \text{sign}(\bar{\rho}_{j\ell}) \max(0, |\bar{\rho}_{j\ell}| - \varpi),$$

and for the hard threshold rule,

$$\mathcal{T}_\varpi[\bar{\rho}_{j\ell}] = \bar{\rho}_{j\ell} 1(|\bar{\rho}_{j\ell}| \geq \varpi).$$

Here  $1(\cdot)$  is the indicator function,  $\text{sign}(\cdot)$  is the sign function, and  $\varpi$  denotes a threshold value that will be specified later.

Methods for estimating a density matrix in physics are often considered by estimating individual matrix elements without studying important matrix properties such as eigenvalues of the estimated density matrix. Artiles, Gill, and Guță (2005) proposed a sieve estimator by projecting a density matrix onto a finite matrix subspace and finding the MLE in the subspace and proved its consistency under trace and Frobenius norms. Butucea, Guță, and Artiles (2007) investigated estimation of the Wigner function, a transformation of the density matrix, by smoothing method and established the asymptotic optimality for the Wigner function estimator. Also see Kerns and Székely (2006) and Székely (2005) for some probability phenomenon analogous to the Wigner function.

### 3.3. Asymptotic theory

We fix some notation. Given a  $p$ -dimensional vector  $\mathbf{x} = (x_1, \dots, x_p)^\dagger$  and a  $p$  by  $p$  matrix  $\mathbf{U} = (U_{j\ell})$ , let

$$\|\mathbf{x}\|_d = \left( \sum_{j=1}^p |x_j|^d \right)^{1/d}, \quad \|\mathbf{U}\|_d = \sup\{\|\mathbf{U}\mathbf{x}\|_d, \|\mathbf{x}\|_d = 1\}, \quad d = 1, 2, \infty.$$

Here we can take  $p = \infty$  for an infinite-dimensional vector or matrix, and then  $\|\mathbf{U}\|_2$  is the square root of the largest eigenvalue of  $\mathbf{U}(\mathbf{U}^\dagger)^*$ ,

$$\|\mathbf{U}\|_1 = \max_{1 \leq \ell \leq p} \sum_{j=1}^p |U_{j\ell}|, \quad \|\mathbf{U}\|_\infty = \max_{1 \leq j \leq p} \sum_{\ell=1}^p |U_{j\ell}|,$$

and  $\|\mathbf{U}\|_2^2 \leq \|\mathbf{U}\|_1 \|\mathbf{U}\|_\infty$ . For symmetric or self-adjoint  $\mathbf{U}$ ,  $\|\mathbf{U}\|_2$  is equal to its largest absolute eigenvalue, and  $\|\mathbf{U}\|_2 \leq \|\mathbf{U}\|_1 = \|\mathbf{U}\|_\infty$ .

We need to impose some technical conditions for the asymptotic theory.

A1. For  $\alpha > 0$  and a constant  $C_1$  free of  $p$ ,

$$\max_{1 \leq j \leq p} \sum_{\ell > p} |\rho_{j\ell}| \leq C_1 p^{-\alpha}, \quad \max_{j > p} \sum_{\ell \geq 1} |\rho_{j\ell}| \leq C_1 p^{-\alpha}.$$

A2. For all  $1 \leq j \leq p$ ,  $\sum_{\ell=1}^p |\rho_{j\ell}|^\delta \leq C_2 \pi(p)$ , where  $0 \leq \delta < 1$ ,  $C_2$  is a constant free of  $p$ , and  $\pi(p)$  is a function of  $p$  with slow growth such as  $\pi(p) = 1$  or  $\log p$ .

Since  $\rho$  is an infinite matrix, we need to control its entries at rows and columns going to infinity as well as to assume sparsity so that it can be consistently estimated. Condition A1 imposes a decay condition on the size of entries as rows and columns go to infinity. As  $\rho$  is semi-positive with unit trace, its entries at large rows and columns must be small. Assumption A1 is a mathematical formulation that controls entries at large rows and columns. Condition A2 is a usual sparse condition in the large matrix estimation literature that assumes a small portion of entries with significantly large magnitude.

Assumptions A1 and A2 are reasonable. Consider the standard quantum states: vacuum state, single photon state, thermal state, coherent state and squeezed state (see Artiles, Gill, and Guță (2005)). For vacuum state and single photon state, the density matrices have respective elements  $\rho_{11} = 1$  and  $\rho_{22} = 1$ , zero elsewhere; for thermal state, the density matrix is a diagonal matrix with diagonal elements  $\rho_{jj} = (1 - e^{-\beta})e^{-j\beta}$  for some parameter  $\beta > 0$ ; for coherent state, the density matrix has elements  $\rho_{j\ell} = e^{-b} b^{j+\ell} (j!\ell!)^{-1/2}$  for some parameter  $b > 0$ ; for squeezed state, the density matrix has elements  $\rho_{j\ell} = c_0 c_1^{j+\ell} h_j(c_2) h_\ell(c_2) (j!\ell!)^{-1/2}$ , where  $c_0, c_1, c_2$  are some constants, and  $h_j$  and  $h_\ell$  are the Hermite polynomials. It is easy to see that vacuum state, single photon state, and thermal state obey A1 and A2. For coherent state, by Stirling's formula we obtain

$$\rho_{j\ell} \sim e^{-b} b^{j+\ell} (2\pi j\ell)^{-1/4} \left(\frac{j}{e}\right)^{-j/2} \left(\frac{\ell}{e}\right)^{-\ell/2} = e^{-b} (2\pi j\ell)^{-1/4} \left(b\sqrt{\frac{e}{j}}\right)^j \left(b\sqrt{\frac{e}{\ell}}\right)^\ell,$$

which decays faster than  $\varsigma^{j+\ell}$  for large  $j$  and  $\ell$ , where  $\varsigma$  is any positive number in  $(0, 1)$ . Thus, it satisfies A1 and A2. As  $h_j(c_2)$  and  $h_\ell(c_2)$  are bounded by  $c_3^j$  and  $c_3^\ell$  for some positive constant  $c_3$ , for squeezed state we have  $|\rho_{j\ell}| \leq c_0(c_1c_3)^{j+\ell}(j!\ell!)^{-1/2}$ , where the upper bound has the same expression as the elements of the density matrix for coherent state, and hence satisfies A1 and A2.

The following theorem establishes the convergence rate for  $\hat{\rho}$ .

**Theorem 1.** *Under A1 and A2, we have*

$$\|\hat{\rho} - \rho\|_2 \leq \|\hat{\rho} - \rho\|_1 = O_P(p^{-\alpha} + \pi(p)\varpi^{1-\delta}),$$

where  $\varpi = \zeta p^{1/4}(\log p/n)^{1/2}$  for some constant  $\zeta$ . In particular for  $\pi(p) \leq \log p$ , if we take  $p = c_0 n^{2(1-\delta)/(4\alpha+1-\delta)}$  with constants  $c_0 > 0$ , then

$$\|\hat{\rho} - \rho\|_2 \leq \|\hat{\rho} - \rho\|_1 = O_P(n^{-2\alpha(1-\delta)/(4\alpha+1-\delta)}[\log n]^{(3-\delta)/2}).$$

Theorem 1 shows that the proposed estimator  $\hat{\rho}$  with the given threshold can be consistent with convergence rate  $n^{-2\alpha(1-\delta)/(4\alpha+1-\delta)}[\log n]^{(3-\delta)/2}$ . In particular, for the case of  $\delta = 0$ ,  $\hat{\rho}$  has a convergence rate  $n^{-2\alpha/(4\alpha+1)} \log^{3/2} n$  under the matrix norms. Estimation of density matrices and the corresponding Wigner functions are studied by, for example, Artiles, Gill, and Guță (2005), Guță and Artiles (2007), and Butucea, Guță, and Artiles (2007) under trace and Frobenius norms. Matrix estimation under these norms is essentially the same as function or vector estimation in nonparametric regression and density estimation, which can be quite different from that under matrix spectral norm (see Cai and Zhou (2012)). Guță and Artiles (2007) proved that for estimating a supersmooth Wigner function, the minimax convergence rate is  $n^{-1/2} \log^{3/2} n$ , which matches the convergence rate of sparse density matrix estimation only in the case of  $\delta = 0$  and  $\alpha \rightarrow \infty$ . The model setting in Guță and Artiles (2007) is the same as in this paper, but the loss used for Wigner function estimation in Guță and Artiles (2007) corresponds to the Frobenius norm for density matrix estimation. While the convergence of a density matrix estimator to the true density matrix in the Frobenius norm is unable to characterize their eigen-behaviors, our asymptotic result in the spectral norm indicates that the eigenvalues of  $\hat{\rho} - \rho$  approach to zero, which implies that the eigenvalues of  $\hat{\rho}$  are close to the true eigenvalues of  $\rho$ .

As discussed in Section 3.2, we estimate the infinite density matrix  $\rho$  through truncating and thresholding. The first part of the convergence rate  $p^{-\alpha} + \pi(p)\varpi^{1-\delta}$  in Theorem 1 is due to truncating, while the other part is attributed to the sparsity imposed on  $\rho$  and the thresholding strategy used in the estimation method. The truncation size  $p$  plays a role in determining the convergence rate similar to function smoothing estimation with orthogonal bases where we select

truncation size to balance the squared bias and variance in order to minimize the mean square error.

In quantum information the closeness of two quantum states is often described by trace-based measures such as trace distance and fidelity. For two Hermitian matrices  $\mathbf{U}$  and  $\mathbf{V}$ , the trace distance and fidelity are defined by, respectively,

$$D(\mathbf{U}, \mathbf{V}) = \text{Tr} \left( \sqrt{(\mathbf{U} - \mathbf{V})^\dagger (\mathbf{U} - \mathbf{V})} \right), \quad F(\mathbf{U}, \mathbf{V}) = \text{Tr} \left( \sqrt{\mathbf{U}^{1/2} \mathbf{V} \mathbf{U}^{1/2}} \right).$$

The matrix norms  $\|\cdot\|_d$  used are induced  $d$ -norms. For example, spectral norm  $\|\cdot\|_2$  corresponds to an induced norm with  $d = 2$ . Trace distance  $D(\mathbf{U}, \mathbf{V})$  is equal to the trace norm (or nuclear norm) of  $\mathbf{U} - \mathbf{V}$ , denoted by  $\|\mathbf{U} - \mathbf{V}\|_*$ . Both spectral norm  $\|\cdot\|_2$  and trace norm  $\|\cdot\|_*$  are the Schatten  $q$ -norms with corresponding  $q = \infty$  and  $q = 1$ , where the Schatten  $q$ -norm is

$$\|\mathbf{U}\|_q = \left( \sum_{j=1}^p |\lambda_j|^q \right)^{1/q},$$

with  $\lambda_j$  the eigenvalues of  $\mathbf{U}$ . The Schatten 2-norm is the Frobenius norm or the Hilbert Schmidt norm. We have

$$2[1 - F(\mathbf{U}, \mathbf{V})] \leq D(\mathbf{U}, \mathbf{V}) \leq 2\sqrt{1 - F^2(\mathbf{U}, \mathbf{V})}, \quad (3.6)$$

$$D(\mathbf{U}, \mathbf{V}) = \|\mathbf{U} - \mathbf{V}\|_* \leq p\|\mathbf{U} - \mathbf{V}\|_2. \quad (3.7)$$

(3.6) indicates that both trace distance and fidelity can be used to measure statistical loss in density matrix estimation. For the density matrix estimator  $\hat{\rho}$  of  $\rho$ , using (3.7) we obtain

$$D(\hat{\rho}, \rho) \leq D(\hat{\rho}, \rho_p) + D(\rho_p, \rho) \leq p\|\hat{\rho} - \rho_p\|_2 + D(\rho_p, \rho),$$

where  $\rho_p$  is the truncation of  $\rho$  that retains only its first  $p$  rows and columns. As in Theorem 1 (and its proof) the main part  $D(\hat{\rho}, \rho_p)$  can be bounded through  $\|\hat{\rho} - \rho_p\|_2$ , which has convergence rate  $\pi(p)\varpi^{1-\delta}$ , while the bias part  $D(\rho_p, \rho)$  caused by the truncation may be controlled through some decaying property of  $\rho$ .

### 3.4. Semi-positive definite estimator of density matrix

True density matrix  $\rho$  is semi-positive with unit trace, but the estimator  $\hat{\rho}$  in (3.5) may not be. Denote by  $\Gamma$  the set of all semi-positive definite matrices with unit trace. We consider the projection of  $\hat{\rho}$  onto  $\Gamma$  to yield a density matrix estimator  $\tilde{\rho}$  that is semi-positive definite and has unit trace: take  $\tilde{\rho}$  to be the matrix in  $\Gamma$  that minimizes the spectral distance to  $\hat{\rho}$ ,

$$\|\tilde{\rho} - \hat{\rho}\|_2 = \min\{\|\check{\rho} - \hat{\rho}\|_2, \check{\rho} \in \Gamma\}. \quad (3.8)$$

The following theorem provides the characterization of  $\tilde{\rho}$ .

**Theorem 2.** *If  $\hat{\rho}$  has an eigen-decomposition*

$$\hat{\rho} = O \text{diag}(\hat{\lambda}_1, \hat{\lambda}_2, \dots, \hat{\lambda}_p) O^\dagger, \tag{3.9}$$

*with eigenvalues  $\hat{\lambda}_1 \geq \hat{\lambda}_2 \geq \dots \geq \hat{\lambda}_p$ , and  $O$  a unitary matrix, then*

$$\tilde{\rho} = O \text{diag}(\tilde{\lambda}_1, \tilde{\lambda}_2, \dots, \tilde{\lambda}_p) O^\dagger, \tag{3.10}$$

*where  $(\tilde{\lambda}_1, \dots, \tilde{\lambda}_p)$  is a solution to the following minimization problem*

$$\min_{\nu_1, \dots, \nu_p} \left\{ \max_{1 \leq j \leq p} |\nu_j - \hat{\lambda}_j|, \nu_1, \dots, \nu_p \geq 0, \sum_{j=1}^p \nu_j = 1 \right\}. \tag{3.11}$$

*Moreover,  $\|\tilde{\rho} - \rho\|_2 \leq 2\|\hat{\rho} - \rho\|_2$ , and  $\tilde{\rho}$  has the same convergence rate as  $\hat{\rho}$ .*

The optimization problem (3.11) may have multiple solutions, and there are no simple closed forms for its solutions, the eigenvalues  $\tilde{\lambda}_j$  of  $\tilde{\rho}$ . Theorem 2 shows that  $\tilde{\rho}$  defined by any solution of (3.11) has the same convergence rate as  $\hat{\rho}$ . Moreover, the proof of Theorem 2 indicates that  $\|\tilde{\rho} - \hat{\rho}\|_2 \leq \|\hat{\rho} - \rho\|_2$ . As Theorem 1 implies that  $\hat{\rho}$  converges to  $\rho$  at the rate  $n^{(1-\delta)/2} [\log n]^{(3-\delta)/2}$ , asymptotically  $\tilde{\rho}$  and  $\hat{\rho}$  are very close.

#### 4. A Simulation Study

We conducted a simulation study to demonstrate the finite sample performances of the proposed density matrix estimators. From (3.1), given a density matrix  $\rho = (\rho_{jl})$  we simulated  $(X_\phi, \phi)$  from a distribution with joint pdf

$$h_\rho(x, \phi) = \frac{1}{\pi} \sum_{j,l=1}^{\infty} \rho_{jl} e_j(x) e_l(x) \cos((j-l)\phi), \quad x \in (-\infty, \infty), \phi \in [0, \pi].$$

We truncated infinite density matrix  $\rho$  by a matrix of size  $p = 16, 64, 128, 256$  to evaluate the joint density function and carry out the simulation. For a given  $p$ , we considered three scenarios:

- (i)  $\rho = \gamma \gamma^\dagger$ ,  $\gamma = (2^{-1/2}, 2^{-1}, \dots, 2^{(1-p)/2}, 2^{(1-p)/2})^\dagger$ ;
- (ii)  $\rho_{jl} = \gamma_{\max(j,l)} 2^{|j-l|}$ ,  $\gamma = (2^{-1}, 2^{-2}, \dots, 2^{1-p}, 2^{1-p})^\dagger$ ;
- (iii)  $\rho = \text{diag}(1/2, 1/4, \dots, 2^{-p+1}, 2^{-p+1})$ .

As described in Section 3.1, the marginal distribution of  $\phi$  is a uniform distribution on  $[0, \pi]$ . Given  $\phi$ , the conditional density function of  $X_\phi$  is

$$g_\rho(x|\phi) = \sum_{j,l=1}^p \rho_{jl} e_j(x) e_l(x) \cos((j-l)\phi), \quad x \in (-\infty, \infty). \tag{4.1}$$

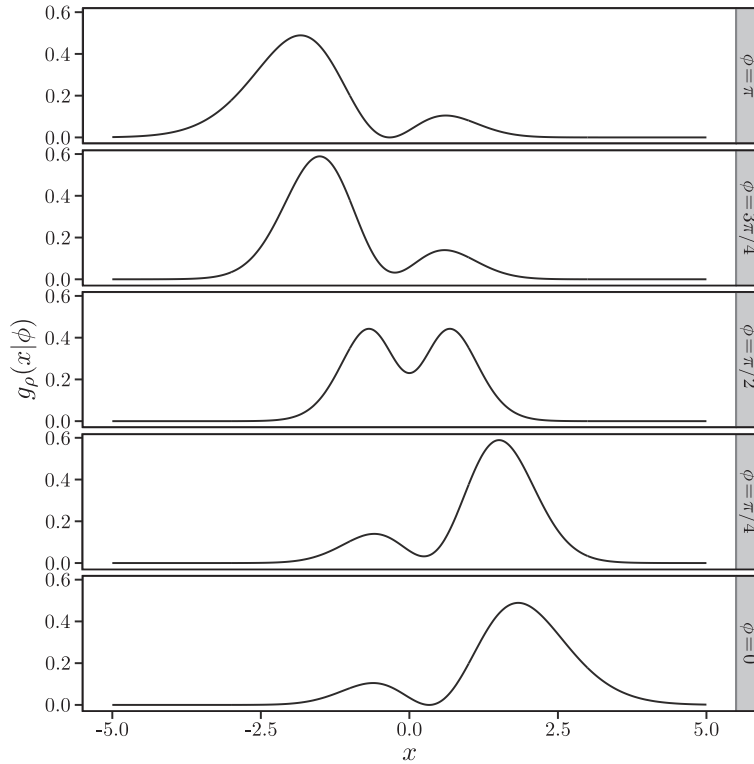


Figure 1. The plots of conditional density function  $g_\rho(x|\phi)$  for five values of  $\phi$  in Scenario (i). The five plots from bottom to top correspond to  $\phi = 0, \pi/4, \pi/2, 3\pi/4, \pi$ , respectively.

We found that numerically  $g_\rho(x|\phi)$  was effectively zero outside the interval  $[-15, 15]$ , and on interval  $[-15, 15]$  we evaluated  $g_\rho(x|\phi)$  at equally-spaced grid points with step size 0.001. The plots of the conditional density functions for the three cases are displayed in Figures 1–3. The plots show that the conditional density functions are bimodal and numerically negligible outside the interval  $[-4, 4]$  for all three cases, and  $X_\phi$  and  $\phi$  are independent for case (iii), but correlated for cases (i) and (ii). The shape patterns in cases (i) and (ii) change along with  $\phi$ , which indicates that the quantum systems exhibit some phase change phenomenon.

To generate random variable  $(X_\phi, \phi)$  from the joint pdf  $h_\rho(x, \phi)$ , we first generated  $\phi$  from the uniform distribution on  $[0, \pi]$ , and with a simulated  $\phi$ , we then simulated  $X_\phi$  from the computed conditional density function  $g_\rho(x|\phi)$ . Repeating the procedure we simulated i.i.d. observations  $(X_{\phi_1}, \phi_1), \dots, (X_{\phi_n}, \phi_n)$  from the bivariate density function  $h_\rho(x, \phi)$  with  $n = 2,000, 5,000$ . Figure 4 provides the scatter plots of the 2,000 simulated data for the three cases. The plots show that the simulated  $X_{\phi_k}$  mostly range from  $-4$  to  $4$  for the three cases,

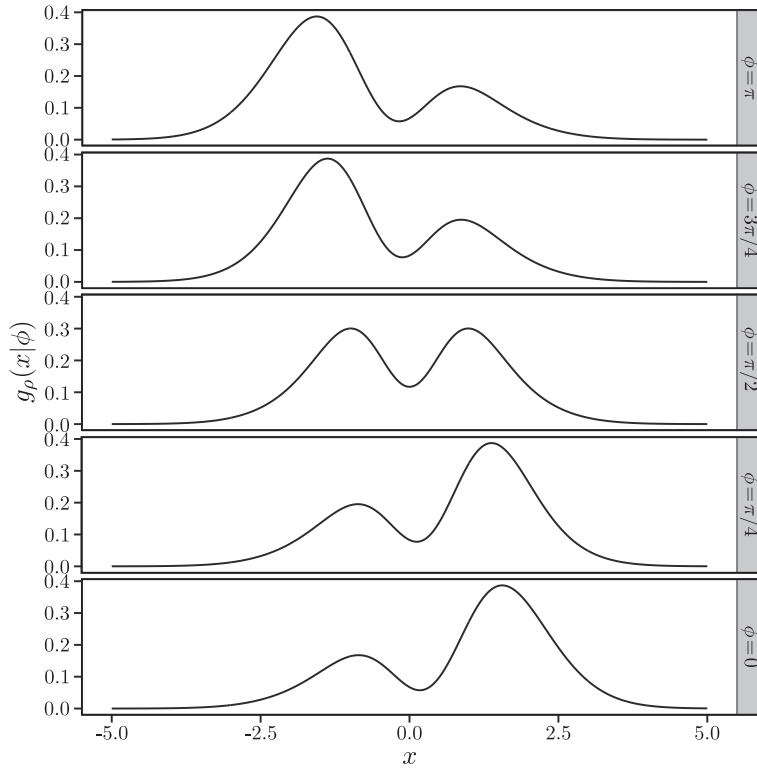


Figure 2. The plots of conditional density function  $g_\rho(x|\phi)$  for five values of  $\phi$  in Scenario (ii). The five plots from bottom to top correspond to  $\phi = 0, \pi/4, \pi/2, 3\pi/4, \pi$ , respectively.

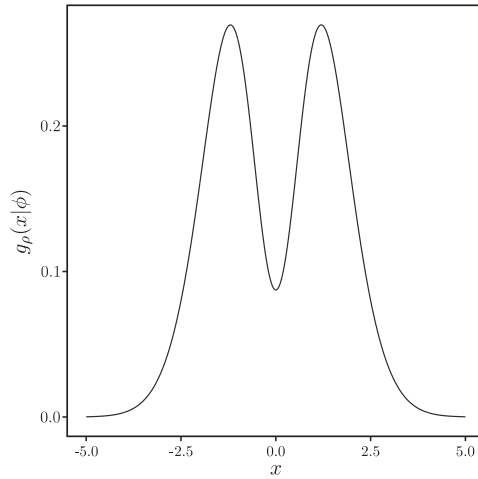


Figure 3. The plot of conditional density function  $g_\rho(x|\phi)$  for any  $\phi$  in Scenario (iii).

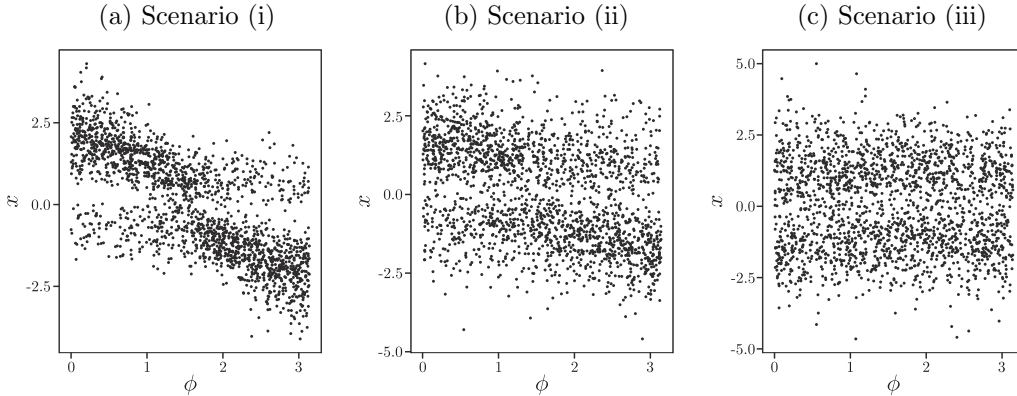


Figure 4. The scatter plots of 2,000 i.i.d. observations generated from the distribution with pdf  $h_\rho(x, \phi)$ . Plots (a), (b) and (c) correspond to Scenarios (i), (ii), (iii), respectively.

and data patterns indicate the dependence of  $X_\phi$  and  $\phi$  for cases (i) and (ii).

With simulated data  $(X_{\phi_1}, \phi_1), \dots, (X_{\phi_n}, \phi_n)$ , according to (3.4) we evaluated each  $\bar{\rho}_{jl}$  as

$$\bar{\rho}_{jl} = \frac{1}{n} \sum_{k=1}^n f_{jl}(X_k) \cos((j-l)\phi_k), \tag{4.2}$$

where we calculated  $f_{jl}(x)$  by a procedure described in Leonhardt et al. (1996, Sec. 5),

$$f_{jl}(x) = f_{lj}(x) = 2x\psi_j(x)\varphi_l(x) - \sqrt{2(j+1)}\psi_{j+1}(x)\varphi_l(x) - \sqrt{2(l+1)}\psi_j(x)\varphi_{l+1}(x),$$

with the procedure for computing  $\psi_j(x)$  and  $\varphi_l(x)$  described below.

With

$$\psi_0(x) = \pi^{-1/4} \exp\left(-\frac{x^2}{2}\right), \quad \psi_1(x) = \pi^{-1/4} \sqrt{2x} \exp\left(-\frac{x^2}{2}\right),$$

we computed  $\psi_j(x)$  from  $\psi_0(x)$  and  $\psi_1(x)$  by the forward recursive formula

$$\psi_j(x) = \frac{1}{\sqrt{j}} \left[ \sqrt{2}x\psi_{j-1}(x) - \sqrt{j-1}\psi_{j-2}(x) \right].$$

We then used a backward recursive formula,

$$\varphi_l(x) = \frac{1}{\sqrt{l+1}} \left[ \sqrt{2}x\varphi_{j+1}(x) - \sqrt{j+2}\psi_{j+2}(x) \right],$$

from  $4\beta$  and  $4\beta - 1$  backward to compute  $\varphi_l(x)$  for  $|x| < a_{4\beta} - (2a_{4\beta})^{-1/3}$ ,  $a_l = \sqrt{2l+1}$ , where  $\beta = 4p$ , and for  $l = 4\beta$  and  $4\beta - 1$ ,

$$\varphi_l = \left( \frac{2}{\pi a_l \sin(t_l)} \right)^{1/2} \sin \left[ \frac{a_l^2}{4} \{ \sin(2t_l) - 2t_l \} + \frac{\pi}{4} \right], \quad t_l = \arccos\left(\frac{x}{a_l}\right);$$

outside the region  $|x| < a_{4\beta} - (2a_{4\beta})^{-1/3}$ , we computed  $\varphi_l(x)$  by the forward recursion,

$$\varphi_0(x) = \pi^{-3/4} x^{-1} \exp\left(\frac{x^2}{2}\right), \quad \varphi_l(x) = \left(\frac{l}{2}\right)^{1/2} x^{-1} \varphi_{l-1}(x).$$

With  $p$  by  $p$  matrix estimator  $\bar{\rho} = (\bar{\rho}_{jl})$ , we applied threshold methodology to  $\bar{\rho}$  and obtained hard and soft threshold density matrix estimators,

$$\hat{\rho}_{jl}^{(hard)} = \bar{\rho}_{jl} 1(|\bar{\rho}_{jl}| \geq \varpi^{(hard)}), \quad \hat{\rho}_{jl}^{(soft)} = \text{sign}(\bar{\rho}_{jl}) \max(0, |\bar{\rho}_{jl}| - \varpi^{(soft)}), \quad (4.3)$$

with  $\varpi^{(hard)}$  and  $\varpi^{(soft)}$  as the threshold values. Threshold  $\varpi$  is a tuning parameter, and we proposed a threshold selection method based on ten-fold cross-validation, as follows.

1. Partition the data randomly into 10 equal-size subsamples, and label the subsamples as  $k = 1, \dots, 10$ .
2. For  $k$  from 1 to 10, use the  $k$ -th subsample as the validation sample and the remaining subsamples as training data.
  - (a) Calculate the density matrix estimator  $\bar{\rho}_k^{(valid)}$  according to (4.2) using the validation sample.
  - (b) Calculate the density matrix estimator  $\hat{\rho}_k^{(train)}$  according to (4.2) using the training data; and then, according to (4.3), threshold it to obtain the threshold estimator  $\hat{\rho}_{\varpi,k}^{(train)}$  with a candidate threshold value  $\varpi$  for either hard or soft threshold rules.
  - (c) Calculate the spectral norm of the difference between  $\hat{\rho}_{\varpi,k}^{(train)}$  and  $\bar{\rho}_k^{(valid)}$  for each candidate  $\varpi$  and  $k = 1, \dots, 10$ .
  - (d) For each candidate  $\varpi$ , evaluate the average objective function for the ten-fold cross-validation

$$\bar{\Lambda}(\varpi) = \sum_{k=1}^{10} \|\hat{\rho}_{\varpi,k}^{(train)} - \bar{\rho}_k^{(valid)}\|_2. \quad (4.4)$$

3. Select  $\varpi$  to minimize  $\bar{\Lambda}(\varpi)$ , and use it as a threshold value for the threshold estimator in (4.3) with the corresponding threshold rule.

For the three scenarios, we ran the ten-fold cross-validation procedure and computed  $\bar{\Lambda}(\varpi)$ . We also used the true density matrix  $\rho$  instead of  $\bar{\rho}_k^{(valid)}$  in the cross-validation algorithm to evaluate the corresponding average objective function, which is denoted by  $\Lambda^*(\varpi)$ . Note that as a counterpart of  $\bar{\Lambda}(\varpi)$ ,  $\Lambda^*(\varpi)$  involves the true density matrix  $\rho$ . Thus we referred  $\Lambda^*(\varpi)$  to as the true average objective function and called the cross-validation procedure that selects a threshold by minimizing  $\Lambda^*(\varpi)$  instead of  $\bar{\Lambda}(\varpi)$  the oracle cross-validation threshold

selection, and the resulting threshold an oracle cross-validation threshold. We compared the selected threshold values based on  $\bar{\Lambda}(\varpi)$  and its true counterpart  $\Lambda^*(\varpi)$  to check the performance of the proposed cross-validation selection. Figures 5-7 plot the average objective function  $\bar{\Lambda}(\varpi)$  and the corresponding true average objective function  $\Lambda^*(\varpi)$  against tuning parameter  $\varpi$  for various combinations of  $(n, p)$  with soft and hard threshold rules. We computed  $\bar{\Lambda}(\varpi)$  and  $\Lambda^*(\varpi)$  and plotted them over many repetitions, and found their shapes and patterns remained similar from repetition to repetition. The plots show that the two curves of  $\bar{\Lambda}(\varpi)$  and  $\Lambda^*(\varpi)$  have global minimizers close to each other. Since the tuning parameter  $\varpi$  is selected by the minimizers, the close minimizers of the two curves indicate the effectiveness of the proposed threshold selection by cross validation. From the figures we see that the curves first drop dramatically to reach their minimal values and then start to rise; as  $p$  increases, the curves tend to be less steep; and when sample size  $n$  increase, the curves become more steep. Since for more steep curves, it is easier to find their minimizers and select the tuning parameters, the plots imply that the performance of the threshold selection method is enhanced for larger  $n$  and worsened for larger  $p$ . Regarding the hard and soft threshold rules, they both work. However, as in the wavelet literature, the curves are much more smooth and sharp around the minima for the soft threshold rule than the hard threshold rule and, as a result, the threshold selection procedure is more stable for the soft threshold rule than the hard threshold rule. In fact, the curves for the hard threshold rule may be non-smooth or even have flat parts. When  $\bar{\Lambda}$  and  $\Lambda^*$  have flat parts around their minima, there are multiple global minimizers, and the tuning parameter is not unique. It indicates the existence of multiple threshold values for the hard threshold rule. Indeed, when there is a gap between those significantly large  $\bar{\rho}_{j\ell}$  (which will be retained by thresholding) and those negligible  $\bar{\rho}_{j\ell}$  (which will be replaced by zero by thresholding), any value in the gap used as a threshold will yield the same estimator  $\hat{\rho}^{(hard)}$  and thus the same MSE.

We evaluated the finite sample performances of the proposed density matrix estimators. For each of the three density matrix cases, we took  $n = 2,000, 5,000$  and  $p = 16, 64, 128, 256$  and computed  $\hat{\rho}$  according to (3.5) with the cross-validation threshold and the oracle cross-validation threshold. We used the spectral norm of  $\hat{\rho} - \rho$  to define the mean square error (MSE). We repeated the whole simulation procedure 200 times and evaluated the MSE of  $\hat{\rho}$  based on 200 repetitions. Tables 1 and 2 report the MSE of  $\hat{\rho}$  for  $n = 2,000, 5,000, p = 16, 64, 128, 256$ , and three scenarios of density matrices for the cross-validation threshold and oracle cross-validation threshold cases, respectively. The simulation results illustrate that for both cross-validation threshold and oracle cross-validation threshold cases, the MSEs of the three estimators all increase as  $p$  increases and

Table 1. The MSEs with standard errors (se) of density matrix estimators given by (4.2) and (4.3) for  $n = 2,000, 5,000, p = 16, 64, 128, 256$ , and Scenarios (i), (ii) and (iii), where the thresholds are selected by the ten-fold cross-validation threshold selection procedure that minimizes the average objective function  $\bar{\Lambda}(\varpi)$  defined in (4.4).

$p$	Estimator	$n = 2,000$ and Scenario			$n = 5,000$ and Scenario		
		(i)	(ii)	(iii)	(i)	(ii)	(iii)
16	$\bar{\rho}$	0.19	0.18	0.18	0.12	0.11	0.11
	se	0.02	0.02	0.02	0.01	0.01	0.01
	$\hat{\rho}^{(soft)}$	0.17	0.12	0.09	0.12	0.08	0.06
	se	0.03	0.02	0.02	0.02	0.01	0.01
	$\hat{\rho}^{(hard)}$	0.17	0.11	0.08	0.11	0.08	0.05
	se	0.03	0.03	0.03	0.02	0.02	0.02
64	$\bar{\rho}$	0.45	0.42	0.41	0.29	0.26	0.26
	se	0.03	0.02	0.02	0.02	0.01	0.01
	$\hat{\rho}^{(soft)}$	0.32	0.20	0.14	0.21	0.13	0.09
	se	0.04	0.03	0.04	0.03	0.02	0.02
	$\hat{\rho}^{(hard)}$	0.27	0.17	0.13	0.17	0.11	0.07
	se	0.05	0.06	0.06	0.03	0.02	0.03
128	$\bar{\rho}$	0.72	0.65	0.64	0.45	0.40	0.40
	se	0.04	0.03	0.03	0.03	0.02	0.02
	$\hat{\rho}^{(soft)}$	0.46	0.27	0.20	0.31	0.18	0.12
	se	0.06	0.04	0.05	0.03	0.03	0.03
	$\hat{\rho}^{(hard)}$	0.37	0.24	0.17	0.23	0.13	0.09
	se	0.08	0.07	0.08	0.04	0.04	0.04
256	$\bar{\rho}$	1.17	1.02	1.01	0.73	0.64	0.62
	se	0.05	0.04	0.04	0.03	0.02	0.02
	$\hat{\rho}^{(soft)}$	0.66	0.39	0.29	0.42	0.27	0.18
	se	0.06	0.07	0.08	0.04	0.04	0.04
	$\hat{\rho}^{(hard)}$	0.52	0.34	0.19	0.32	0.16	0.12
	se	0.12	0.13	0.10	0.07	0.06	0.06

decrease as  $n$  increases; both  $\hat{\rho}^{(soft)}$  and  $\hat{\rho}^{(hard)}$  have much smaller MSEs than  $\bar{\rho}$  for  $p = 64, 128, 256$ , while most of their MSEs are comparable for  $p = 16$ ; the MSE improvements of  $\hat{\rho}^{(soft)}$  and  $\hat{\rho}^{(hard)}$  over  $\bar{\rho}$  get larger as  $p$  increases;  $\hat{\rho}^{(hard)}$  is better than  $\hat{\rho}^{(soft)}$  in terms of MSE. Comparing Tables 1 and 2, we found that, as expected, the oracle cross-validation threshold yields smaller and slightly more stable MSE than the cross-validation threshold, and the ratios of MSEs with the oracle cross-validation threshold and the corresponding MSEs with the cross-validation threshold increase in  $n$  but decrease in  $p$ , with the MSE ratios ranging from about 95% to 70% for the considered cases. The MSE simulation results further show the reasonably good performance of the proposed cross-validation threshold selection procedure indicated by Figures 5–7. We also

Table 2. The MSEs with standard errors (se) of density matrix estimators given by (4.2) and (4.3) for  $n = 2,000, 5,000$ ,  $p = 16, 64, 128, 256$ , and Scenarios (i), (ii) and (iii), where the thresholds are selected by the oracle cross-validation threshold selection procedure that minimizes the true average objective function  $\Lambda^*(\varpi)$ .

$p$	Estimator	$n = 2,000$ and Scenario			$n = 5,000$ and Scenario		
		(i)	(ii)	(iii)	(i)	(ii)	(iii)
16	$\hat{\rho}_*^{(soft)}$	0.16	0.11	0.07	0.11	0.08	0.05
	se	0.02	0.02	0.01	0.01	0.01	0.01
	$\hat{\rho}_*^{(hard)}$	0.16	0.10	0.06	0.10	0.07	0.04
	se	0.02	0.02	0.02	0.01	0.01	0.01
64	$\hat{\rho}_*^{(soft)}$	0.29	0.18	0.10	0.20	0.12	0.07
	se	0.03	0.02	0.02	0.02	0.01	0.01
	$\hat{\rho}_*^{(hard)}$	0.24	0.14	0.09	0.16	0.10	0.06
	se	0.03	0.03	0.03	0.02	0.01	0.01
128	$\hat{\rho}_*^{(soft)}$	0.37	0.22	0.13	0.26	0.16	0.08
	se	0.03	0.02	0.02	0.02	0.01	0.01
	$\hat{\rho}_*^{(hard)}$	0.30	0.18	0.12	0.19	0.11	0.07
	se	0.04	0.03	0.02	0.02	0.01	0.02
256	$\hat{\rho}_*^{(soft)}$	0.48	0.27	0.16	0.33	0.19	0.10
	se	0.03	0.02	0.02	0.02	0.01	0.01
	$\hat{\rho}_*^{(hard)}$	0.37	0.21	0.13	0.25	0.13	0.09
	se	0.04	0.02	0.03	0.03	0.03	0.03

checked the finite sample performances of semi-positive definite estimator  $\tilde{\rho}$  defined in (3.8). The procedure described by (3.9)–(3.11) was applied to threshold estimators  $\hat{\rho}^{(soft)}$  and  $\hat{\rho}^{(hard)}$  in (4.3) and obtain, respectively,  $\tilde{\rho}^{(soft)}$  and  $\tilde{\rho}^{(hard)}$ , which are semi-positive estimators with unit trace. Here the threshold values for  $\tilde{\rho}^{(soft)}$  and  $\tilde{\rho}^{(hard)}$  were selected by the ten-fold cross-validation method with  $\hat{\rho}$  replaced by  $\tilde{\rho}$ . As in Table 1, for each combination of the three density matrix cases,  $n = 2,000, 5,000$  and  $p = 16, 64, 128, 256$ , the MSEs of  $\tilde{\rho}^{(soft)}$  and  $\tilde{\rho}^{(hard)}$  were computed and reported in Table 3. Tables 1 and 3 indicate that  $\tilde{\rho}^{(soft)}$  and  $\tilde{\rho}^{(hard)}$  have, respectively, comparable performances with or slightly better performances than  $\hat{\rho}^{(soft)}$  and  $\hat{\rho}^{(hard)}$  in terms of MSE. Overall the simulation study conforms with the theoretical findings. For small  $p$ , the density matrices are of small size,  $\bar{\rho}$  is a very good estimator, and there may not be much room for improvement. As  $p$  gets large, we need to estimate density matrices of large size. Like sample covariance matrix estimator,  $\bar{\rho}$  is no longer consistent and performs poorly for large  $p$ . The proposed estimators  $\hat{\rho}$  and  $\tilde{\rho}$  are consistent, and their finite sample performances are much better than that of  $\bar{\rho}$ . Moreover, while  $\hat{\rho}$  and  $\tilde{\rho}$  are comparable,  $\tilde{\rho}$  has an advantage of being a semi-positive definite matrix with unit trace.

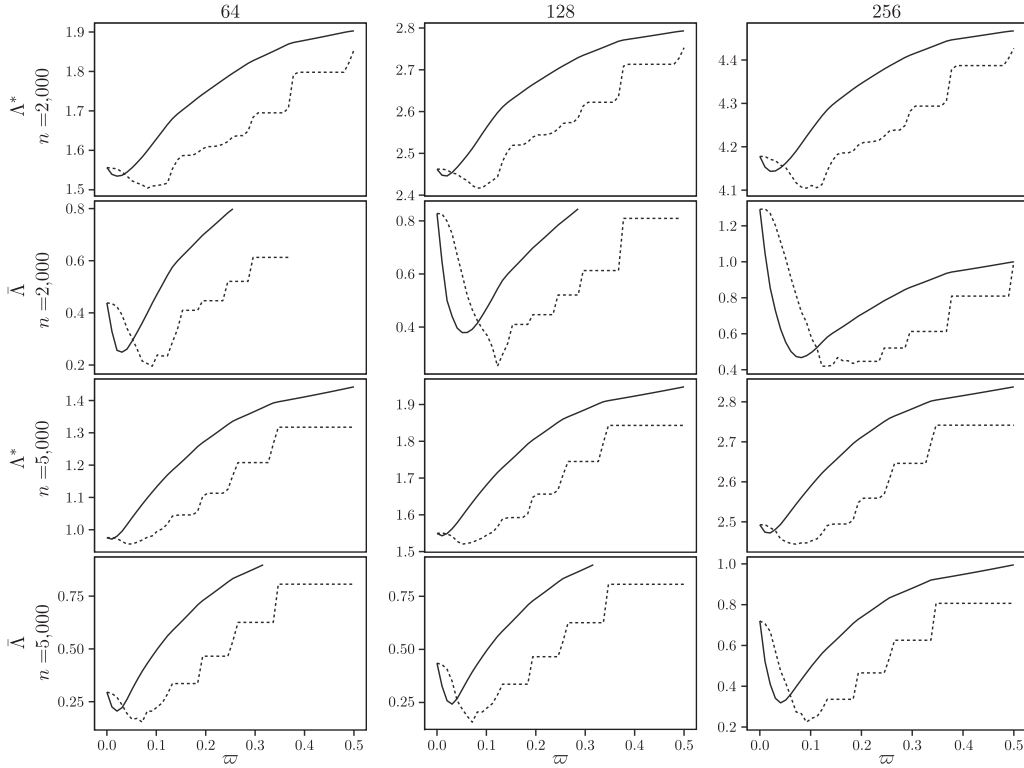


Figure 5. The plots of curves  $\bar{\Lambda}(\varpi)$  and  $\Lambda^*(\varpi)$  in Scenario (i) for various combinations of  $n$ ,  $p$ , and threshold rules. The solid and dot curves in all plots stand for the soft and hard threshold rules, respectively; the plots in the three columns are for  $p = 64, 128, 256$ , respectively; and the plots in the four rows correspond to the combinations of  $(\Lambda^*, n = 2,000)$ ,  $(\bar{\Lambda}, n = 2,000)$ ,  $(\Lambda^*, n = 5,000)$ , and  $(\bar{\Lambda}, n = 5,000)$ , respectively.

### 5. Concluding Remarks

Homodyne detection has been developed to produce data measurements for physical systems in quantum optics, and quantum homodyne tomography is used to confirm certain states of light for the study of quantum computation, quantum information and quantum cryptography. We have proposed statistical methodologies to directly estimate density matrices for the quantum systems. The estimation methods can be implemented by the following procedure: (i) construct  $(\bar{\rho}_{j\ell})$  as described by (3.4); (ii) threshold  $(\bar{\rho}_{j\ell})$  to compute  $\hat{\rho}$  according to (3.5); (iii) evaluate  $\tilde{\rho}$  by (3.10) and (3.11). We have obtained the convergence rates of the proposed density matrix estimators under the spectral norm and conducted simulations to illustrate the finite sample performances of the estimators.

While the proposed methodologies yield new density matrix estimators with

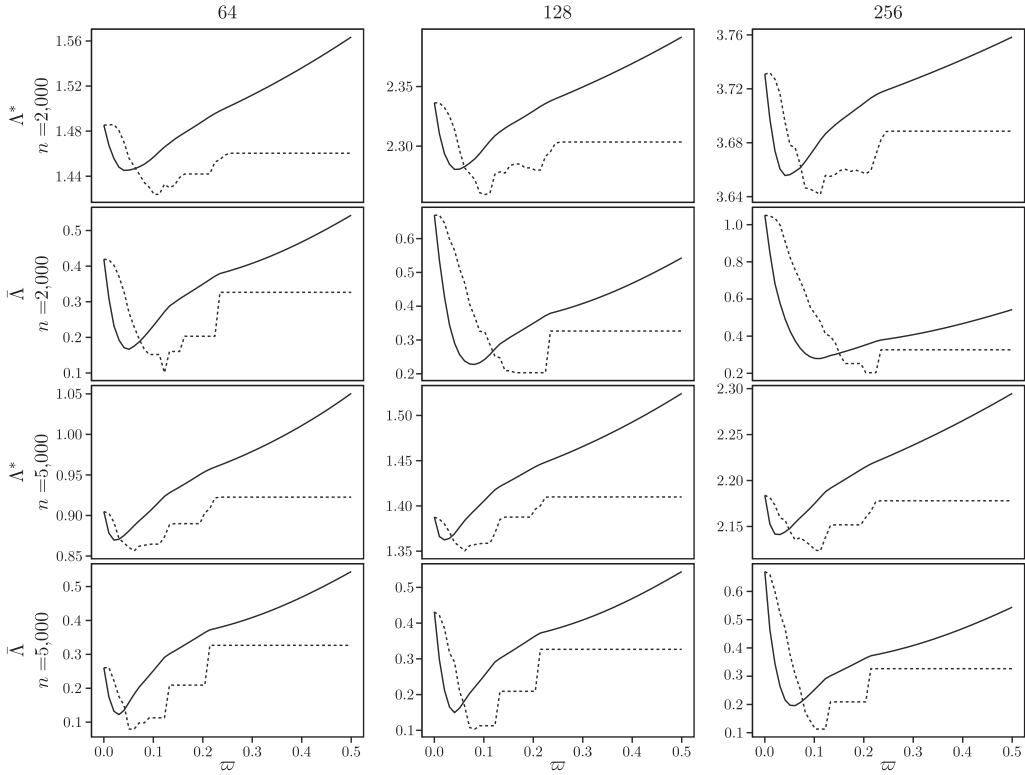


Figure 6. The plots of curves  $\bar{\Lambda}(\varpi)$  and  $\Lambda^*(\varpi)$  in Scenario (ii) for various combinations of  $n$ ,  $p$ , and threshold rules. The solid and dot curves in all plots stand for the soft and hard threshold rules, respectively; the plots in the three columns are for  $p = 64, 128, 256$ , respectively; and the plots in the four rows correspond to the combinations of  $(\Lambda^*, n = 2,000)$ ,  $(\bar{\Lambda}, n = 2,000)$ ,  $(\Lambda^*, n = 5,000)$ , and  $(\bar{\Lambda}, n = 5,000)$ , respectively.

good theoretical and numerical properties, we leave some open issues and topics for future research. For example, in Section 3.1 we consider quantum homodyne tomography in an idealized set-up by assuming that there is no loss in the detection process. In experiments we may need to take into account such losses as mode mismatching and failure of detectors in the detection process. In other words, the quantum homodyne detectors have efficiency smaller than one. We need to modify the model set-up and the distribution results (3.1) and (3.2) through a single efficiency coefficient (see Alquier, Meziani, and Peyré (2013) Artiles, Gill, and Guță (2005), Aubry, Butucea, and Meziani (2009), Butucea, Guță, and Artiles (2007), and Leonhardt (1997)), then study the density matrix estimation problem for noisy data in quantum homodyne tomography. In step (ii) of above implementation procedure we may choose a threshold value by the

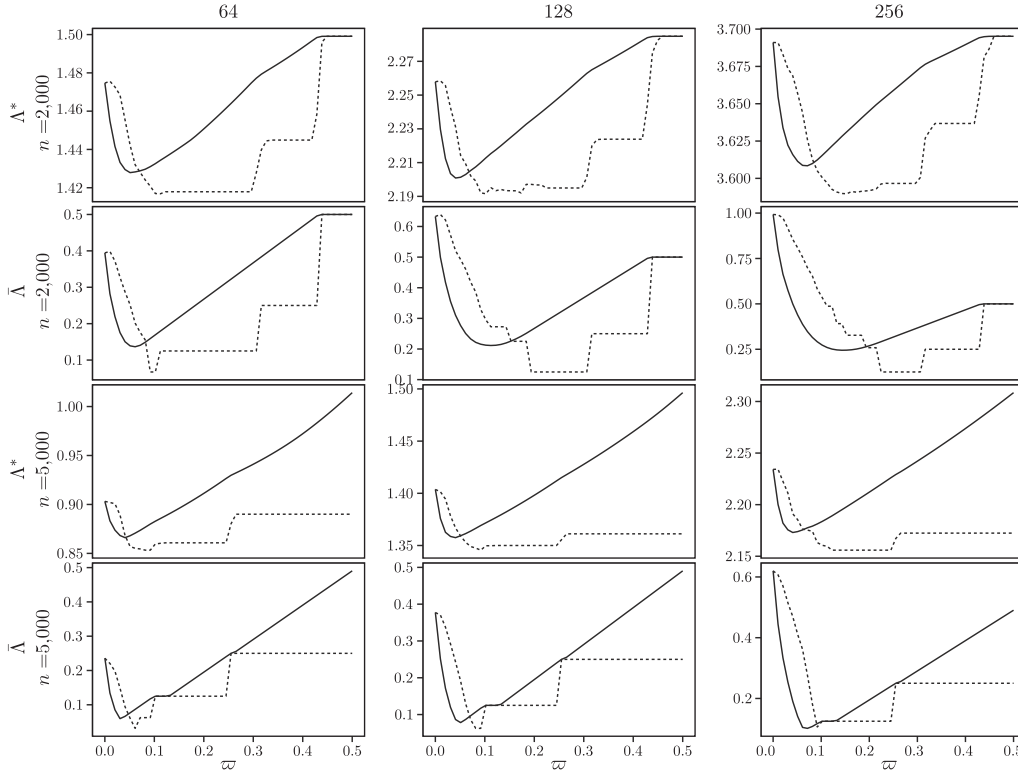


Figure 7. The plots of curves  $\bar{\Lambda}(\varpi)$  and  $\Lambda^*(\varpi)$  in Scenario (iii) for various combinations of  $n$ ,  $p$ , and threshold rules. The solid and dot curves in all plots stand for the soft and hard threshold rules, respectively; the plots in the three columns are for  $p = 64, 128, 256$ , respectively; and the plots in the four rows correspond to the combinations of  $(\Lambda^*, n = 2,000)$ ,  $(\bar{\Lambda}, n = 2,000)$ ,  $(\Lambda^*, n = 5,000)$ , and  $(\bar{\Lambda}, n = 5,000)$ , respectively.

cross-validation method described in Section 4, but a method for selecting truncation size is needed. As discussed in Section 3.3, we may theoretically select the truncation size to minimize the mean square error. However it is desirable to have a data dependent method for the truncation size selection. One theoretical problem is to investigate optimal density matrix estimation. This paper considers density matrix estimators with a universal threshold. Although the proposed density matrix estimators enjoy good convergence rates, it is not clear that they are optimal. For a decay density matrix, we may need to threshold entries more harshly as rows and columns increase. Perhaps the adaptive approach considered in Cai and Liu (2011) for large covariance matrix estimation can be adopted to construct density matrix estimators with individual thresholds to account for heterogeneity among the entries of the true density matrix, and to study the

Table 3. The MSEs with standard errors (se) of semi-positive definite density matrix estimators defined in (3.8) for  $n = 2,000, 5,000$ ,  $p = 16, 64, 128, 256$ , and Scenarios (i), (ii) and (iii).

$p$	Estimator	$n = 2,000$ and Scenario			$n = 5,000$ and Scenario		
		(i)	(ii)	(iii)	(i)	(ii)	(iii)
16	$\tilde{\rho}^{(soft)}$	0.17	0.11	0.07	0.12	0.08	0.05
	se	0.03	0.02	0.02	0.02	0.01	0.01
	$\tilde{\rho}^{(hard)}$	0.17	0.11	0.07	0.11	0.07	0.05
	se	0.03	0.02	0.03	0.02	0.02	0.02
64	$\tilde{\rho}^{(soft)}$	0.34	0.19	0.13	0.23	0.13	0.08
	se	0.03	0.02	0.03	0.02	0.01	0.02
	$\tilde{\rho}^{(hard)}$	0.27	0.15	0.12	0.18	0.10	0.07
	se	0.04	0.04	0.05	0.03	0.02	0.03
128	$\tilde{\rho}^{(soft)}$	0.44	0.24	0.17	0.33	0.17	0.11
	se	0.03	0.02	0.03	0.03	0.02	0.02
	$\tilde{\rho}^{(hard)}$	0.35	0.21	0.15	0.24	0.13	0.09
	se	0.06	0.05	0.06	0.04	0.03	0.04
256	$\tilde{\rho}^{(soft)}$	0.52	0.28	0.21	0.40	0.22	0.15
	se	0.02	0.02	0.04	0.02	0.02	0.03
	$\tilde{\rho}^{(hard)}$	0.45	0.27	0.17	0.32	0.15	0.12
	se	0.06	0.06	0.07	0.05	0.04	0.05

optimal convergence rate in density matrix estimation.

### Acknowledgements

Wang's research was partially supported by NSF grants DMS-105635 and DMS-1265203. The authors thank the Editor, an associate editor, and two referees for comments and suggestions, which led to significant improvements in both the substance and presentation of the paper.

### References

- Alquier, P., Meziani, K. and Peyré, G. (2013). Adaptive estimation of the density matrix in quantum homodyne tomography with noisy data. arXiv:1301.7644v2.
- Aubry, J. M., Butucea, C. and Meziani, K. (2009). State estimation in quantum homodyne tomography with noisy data. *Inverse Problem* **25**, 015003(22pp).
- Artiles, L. M., Gill, R. D., and Guță, M. I. (2005). An invitation to quantum tomography. *J. Roy. Statist. Soc. Ser. B* **67**, 109-134.
- Barndorff-Nielsen, O. E., Gill, R. and Jupp, P. E. (2003). On quantum statistical inference (with discussion). *J. R. Statist. Soc. Ser. B* **65**, 775-816.
- Bickel, P. J. and Levina, E. (2008). Covariance regularization by thresholding. *Ann. Statist.* **36**, 2577-2604.
- Butucea, C., Guță, M. and Artiles, L. (2007). Minimax and adaptive estimation of the Wigner function in quantum homodyne tomography with noisy data. *Ann. Statist.* **35**, 465-494.

- Cai, T. and Liu, W. (2011). Adaptive thresholding for sparse covariance matrix estimation. *J. Amer. Statist. Assoc.* **106**, 672-684.
- Cai, T. and Zhou, H. (2012). Optimal rates of convergence for sparse covariance matrix estimation. *Ann. Statist.* **40**, 2389-2420.
- D'Ariano, G. M., Leonhardt, U., and Paul, H. (1995). Homodyne detection of the density matrix of the radiation field. *Phys. Rev. A*, R1801-1804.
- Gill, R. and Guță, M. (2003). An invitation to quantum tomography. Eurandom report 2003-005. Online first: DOI 10.1007/s002090100316. arXiv:quant-ph/0303020v2 31 May 2004.
- Guță, M. and Artiles, L. (2007). Minimax estimation of the Wigner function in quantum homodyne tomography with ideal detectors. *Math. Methods Statist.* **16**, 1-15.
- Holevo, A. S. (1982). Probabilistic and Statistical Aspects of Quantum Theory. North-Holland, Amsterdam.
- Kerns, J. and Székely, G. J. (2006). Finite exchangeability. *J. Theoret. Probab.* **19**, 589-608.
- Leonhardt, U. (1997). *Measuring the Quantum State of Light*. Cambridge University Press.
- Leonhardt, U., Paul, H. and D'Ariano, G. M. (1995). Tomographic reconstruction of the density matrix via pattern functions. *Phys. Rev. A* **52**, 4899-4907.
- Leonhardt, U., Munroe, M., Kiss, T., Richter, Th., and Raymer, M. G. (1996). Sampling of photon statistics and density matrix using homodyne detection. *Optics Communications* **127**, 144-160.
- Sakurai, J. J. (1995). *Modern Quantum Mechanics*. Addison-Wesley, Reading, Massachusetts.
- Székely, G. J. (2005). Negative probabilities in finance. *Wilmott J. of Quantitative Finance*, 66-68.
- Tao, M., Wang, Y., and Zhou, H. H. (2013). Optimal sparse volatility matrix estimation for high dimensional Itô processes with measurement errors. *Ann. Statist.* **41**, 1816-1864.
- Wang, Y. (2011). Quantum Monte Carlo simulation. *Ann. Appl. Statist.* **5**, 669-683.
- Wang, Y. (2012). Quantum computation and quantum information. *Statist. Sci.* **27**, 373-394.
- Wang, Y. (2013). Asymptotic equivalence of quantum state tomography and noisy matrix completion. *Ann. Statist.* **41**, 2462-2504.
- Wang, Y. and Zou, J. (2010). Vast volatility matrix estimation for high-frequency financial data. *Ann. Statist.* **38**, 943-978.

Department of Statistics, University of Wisconsin-Madison, 1300 University Avenue, Madison, WI 53706, USA.

E-mail: yzwang@stat.wisc.edu

Department of Statistics, University of Wisconsin-Madison, 1300 University Avenue, Madison, WI 53706, USA.

E-mail: chenlian@stat.wisc.edu

(Received October 2013; accepted May 2014)